AGU ADVANCING EARTH AND SPACE SCIENCES

Geophysical Research Letters

RESEARCH LETTER
10.1029/2024GL109774

Special Collection:
Land-atmosphere coupling: measurement, modelling and analysis

First Assessment of Cloud-Land Coupling in LASSO Large-Eddy Simulations

Haipeng Zhang[1,2], Tianning Su[1,2,3], Youtong Zheng[4,5], and Zhanqing Li[1,2]

[1]Department of Atmospheric and Oceanic Science, University of Maryland, College Park, MD, USA, [2]Earth System Science Interdisciplinary Center, University of Maryland, College Park, MD, USA, [3]Lawrence Livermore National Laboratory, Livermore, CA, USA, [4]Department of Earth and Atmospheric Science, University of Houston, Houston, TX, USA, [5]Institute of Climate and Atmospheric Science, University of Houston, Houston, TX, USA

Key Points:

- Observed cloud-land coupling has notable diurnal variations but is inadequately simulated by Large-Eddy Simulations (LESs)
- LESs overestimate the frequency and vertical extent of coupled cumuli in the afternoon
- These overestimations by LESs are related to the misrepresentation of triggering shallow convection

Supporting Information:

Supporting Information may be found in the online version of this article.

Correspondence to:

Z. Li and T. Su,
zhanqing@umd.edu;
su10@llnl.gov

Citation:

Zhang, H., Su, T., Zheng, Y., & Li, Z. (2024). First assessment of cloud-land coupling in LASSO Large-Eddy Simulations. *Geophysical Research Letters*, *51*, e2024GL109774. https://doi.org/10.1029/2024GL109774

Received 12 APR 2024
Accepted 3 JUL 2024

Abstract To enhance our understanding of cloud simulations over land, this study provides the first assessment of coupling between cloud and land surface in the Large-Eddy Simulation (LES) Atmospheric Radiation Measurement Symbiotic Simulation and Observation (LASSO) activity for the shallow convection scenario. The analysis of observation data reveals a diurnal cycle of cloud-land coupling, which co-varies with surface fluxes. However, coupled (or decoupled) cumulus clouds are inadequately simulated, manifesting as a too-high (or low) occurrence frequency during the afternoon. This discrepancy is mirrored by the overestimated cloud liquid water path and cloud-top height. These overestimations are linked to the overpredicted boundary-layer development and the easier trigger of shallow convection misrepresented in LES runs. Our study underscores the need to improve the representations of boundary-layer processes and cloud-land interactions within LES to better simulate shallow clouds in the future.

Plain Language Summary Cloud-surface coupling is crucial in weather and climate predictions, yet its processes, particularly over the land surface, remain poorly understood. This study examined the evolution of coupled cloud occurrence frequency and cloud macro-physical properties [e.g., cloud fraction, liquid water path (LWP), and cloud-top height (CTH)] in LASSO Large-Eddy Simulations (LESs) for 77 shallow convection case days against observations. We found that LES runs erroneously simulate a too-high occurrence frequency of coupled cumulus clouds during the afternoon. In accord with that, shallow convection development is also markedly overestimated during the same period, manifested by overestimated cloud LWP and CTH. These errors are possibly linked to the misrepresentation of a key physical process, namely, the shallow convective trigger, which needs to be improved to achieve more accurate cloud simulations.

1. Introduction

Land-atmosphere interactions play a crucial role in the weather and climate system (Catalano et al., 2016; Dickinson, 1995; Entekhabi, 1995). Through fluxes of moisture and heat at the Earth's surface, land-atmosphere interactions affect the planetary boundary layer (PBL) temperature, moisture, precipitation, and cloud properties, which in turn affect downward radiative fluxes reaching the Earth's surface (Qian et al., 2013; Santanello et al., 2018; Zhang & Klein, 2010, 2013) The coupling between the surface and low-level clouds is a crucial aspect of land-atmosphere interactions.

Enhancing the understanding of cloud-surface coupling is fundamental to improving representations of PBL processes and cloud properties in numerical models. The impact of cloud-surface coupling states on boundary-layer clouds was recently examined by Su et al. (2023), who found that the coupled cloud-surface is conducive to the PBL morning transition from a stable to unstable layer, whereas the decoupled system tends to prolong the persistence of the stable layer, thereby delaying the transition. Meanwhile, cloud-surface coupling is significant to cloud formation and development. By mediating the moisture and energy budget of the boundary layer, the coupling of low clouds with the surface affects boundary-layer turbulent mixing, cloud-top entrainment, precipitation, and related processes, which control cloud development (Dussen et al., 2014, 2015; Sandu et al., 2010; H. Zhang et al., 2023; Y.-T. Zheng, Zhang, & Li, 2021, Zheng, Zhang, Rosenfeld, et al., 2021). The coupling-induced changes in these boundary-layer dynamic and thermodynamic characteristics also possibly influence the sources and sinks of cloud condensation nuclei and then low clouds via aerosol-cloud interactions (Su, Li, Henao, et al., 2024; Wang et al., 2011). The physics of cloud-surface coupling has been mostly investigated over the oceans. For instance, during the stratocumulus-to-cumulus transition where cloud decks advect

toward warmer water, several mechanisms can cause the decoupling of clouds from the surface, like enhanced entrainment warming (Bretherton & Wyant, 1997), precipitation-induced PBL stabilization (Nicholls, 1984), and daytime decoupling by solar radiation that counterbalances cloud-top radiative cooling (Nicholls & Leighton, 1986). In contrast, when cloud decks move toward colder water, surface cooling leads to cloud decks being completely decoupled from the surface by stabilizing the surface-atmosphere interface (Y.-T. Zheng, Zhang, Rosenfeld, et al., 2021). Despite numerous advances in marine-cloud-surface coupling, the mechanisms of cloud-land coupling remain less understood, partly due to more complex surface conditions (e.g., large heterogeneities in surface heat fluxes).

The U.S. Southern Great Plains (SGP) has been a hotspot region for studying land-atmosphere interactions (e.g., Tang et al., 2018; Trier et al., 2011; Y. Zheng et al., 2015), due to its long-term high-quality observations of a wide variety of measurements that fully characterize both the atmosphere and the surface. By providing high-quality initial profiles and forcings, these observations allow for high-resolution simulations of shallow cumulus cases at the SGP site, so-called the Large-Eddy Simulation (LES) Atmospheric Radiation Measurement (ARM) Symbiotic Simulation and Observation (LASSO) activity, which offer a complete and physically consistent picture of the atmospheric state (Gustafson, Vogelmann, Li, et al., 2020). With fine resolutions, LASSO LES simulations help enhance a process-level understanding of cloud and boundary layer processes, such as the coupling of clouds with the land surface.

While we have examined the cloud-surface coupling relationship using observation data over both oceans (Y.-T. Zheng, Zhang, & Li, 2021; Zheng, Zhang, Rosenfeld, et al., 2021) and land (Su et al., 2023; Su, Li, Zhang, et al., 2024), understanding the driving mechanisms and underlying processes requires model simulations, most suitably by the LASSO LES, which to date have not been done. Gustafson, Vogelmann, Li, et al. (2020) have compared simulated shallow cloud fields against observations, revealing significant challenges for LES in accurately simulating the diurnal cycle of shallow cumuli, for example, failing to capture the peak in cloud fraction and substantially underestimating cloud fraction in the afternoon. Moreover, they highlighted the significance of large-scale forcing on cloud simulation throughout the day. Detailed comparisons of cloud fraction, liquid water path (LWP), and cloud-base height (CBH) were archived in LASSO bundles (Gustafson, Vogelmann, Cheng, et al., 2020). Despite these advancements, cloud-land coupling processes in LASSO LES simulations have not yet been evaluated. To fill this gap, our investigation assesses the representation of cloud-land coupling in LES simulations and its consequential impact on cloud macro-physical properties, revealing the crucial role of cloud-land coupling in the simulations. Such an examination is crucial for understanding the physics of cloud-land coupling and for improving shallow cloud simulations in future LASSO experiments.

2. Methodology

2.1. LASSO LES Simulation

The LASSO project was designed to complement the U.S. Department of Energy (DOE) ARM program's extensive suite of measurements, helping bridge the scale gap between ARM observations and models (Gustafson, Vogelmann, Li, et al., 2020). For example, LASSO LES cases have demonstrated their usefulness in parameterization development (Angevine et al., 2018). LASSO keeps adding shallow cumulus cases over land at the ARM SGP site, culminating in ensemble simulations for 95 case days from 2015 to 2019 (Gustafson, Vogelmann, Cheng, et al., 2020; Sisterson et al., 2016). Simulation results are sensitive to the initial and boundary conditions and advection terms supplied to the LES (Basu et al., 2008). LASSO addresses this issue by using different large-scale forcings for each case day, thus producing numerous ensemble members to explore possible correct solutions (Gustafson, Vogelmann, Li, et al., 2020, Gustafson, Vogelmann, Cheng, et al., 2020). In addition to forcing data sets, model settings, such as domain size and microphysics schemes, are also varied to increase the possibility of correct results.

LASSO has conducted multiple sets of simulations for 95 case days, each identified by a unique ID number and featuring different large-scale forcings. It is noted that, in one simulation set, the model configurations (e.g., large-scale forcing, microphysics scheme, and domain size) for the 18 case days in 2015–2016 significantly differ from the rest in 2017–2019. To ensure consistent modeling setups across cases, we focused our analysis on the 77 case days from 2017 to 2019. We chose the ID5 data set to examine the performance of LES in simulating cloud-land coupling. This set of simulations for the selected case days was run using the Weather and Research Forecasting LES model, initialized with 12 UTC radiosonde soundings from the Central Facility (Gustafson, Vogelmann,

Cheng, et al., 2020). The large-scale forcings were specified by the European Center for Medium-Range Weather Forecasts (ECMWF) forecasts (with a forcing scale of 114 km in 2017–2018 and 413 km in 2019), and surface forcings were derived from the observationally based ARM constrained variational analysis, known as VARANAL products (Xie et al., 2004). The domain size was set to 25 km, and the Thompson scheme was adopted for microphysics. Each simulation was conducted for 15 hr with a model output frequency of every 10 min and a vertical grid spacing of 30 m (up to 5 km). We also examined other sets of simulations (ID1-4), driven by different forcings: no forcing, VARANAL300, ECMWF16, and ECMWF413, where the number denotes the forcing scale. These sets exhibit similar results to ID5 (see Figures S1-2 in Supporting Information S1), suggesting no significant influence of large-scale forcings on our main results. The detailed model configurations for the selected case days in ID1-5 were archived in Zhang et al. (2024).

The first several hours of the simulations (i.e., in the early morning) represent the transient transition toward a spun-up model state and may not be fully representative of the model behavior. Therefore, it is important to bear in mind that our evaluations during these early hours are subject to spin-up effects.

2.2. Observations at the SGP Site

For model assessment, this study utilizes the comprehensive cloud, PBL, and meteorological data sets measured at the SGP site from 2017 to 2019, matching the 77 case days. These data sets provide high-frequency cloud macro-physical properties such as cloud fraction and LWP, as well as PBL height (planetary boundary-layer height (PBLH)), lifted condensation level (LCL), and surface fluxes, either directly or through derived ways.

The observed cloud fraction (15-min resolution) is estimated through cloud occurrence frequency measured by vertically pointing lidar and radar and sampled in time from the ARM Active Remote Sensing of Clouds (ARSCL) Value-Added Product (Clothiaux et al., 2000). In LES runs, cloud fraction is derived from grid cells with the sum of the cloud and rainwater mixing ratios greater than 10^{-7} kg/kg (Gustafson et al., 2018). For both observations and LES runs, boundary-layer cloud fractions [called low-cloud fraction (LCF) in our study] are calculated by a cumulative frequency of 15-min cloud occurrences, as identified by ARSCL below 5 km (Gustafson et al., 2018). CBH is determined as the lowest altitude with a cloud fraction greater than zero. Cloud-top height (CTH) is defined as the point at which the cloud fraction reduces to zero for the first time when ascending from the cloud base. Clouds spotted above are not considered here. However, cloud masks derived from ARSCL suffer from observation uncertainty. Fairless et al. (2021) demonstrated that ARSCL retrievals are prone to contamination above the cloud base from insects. These retrievals overestimated CTHs compared to the Clouds Optically Gridded by Stereo (COGS) product that is not susceptible to such contamination by using stereo photogrammetry to identify three-dimensional cloud volumes (Romps & Öktem, 2018). Note that COGS is only available for the 2018 and 2019 LASSO cases since the stereo cameras used for observations were installed in 2018. Our analysis of 2018–2019 LASSO case days supports their findings, showing a systematic overestimation in CTH over time in ARSCL (Figure S3 in Supporting Information S1). The impact of this bias in ARSCL on our results is discussed in Section 3.2.

The observed in-cloud LWP (10-min resolution) is based on microwave-radiometer-only retrievals from the two-channel microwave radiometer (Turner et al., 2007). For LES runs, the simulated in-cloud domain-averaged LWP is computed by taking LWP columns with values greater than 3 g/m^2 (Gustafson, Vogelmann, Cheng, et al., 2020).

The high-resolution (10-min) PBLH is estimated from micropulse lidar data using the function of signal gradient and wavelet covariance transform obtained from backscatter signals (Su et al., 2020). Complementing the lidar-based approach, the PBLH is also determined over the SGP site using the method proposed by Liu and Liang (2010), which relies on vertical thermodynamic profiles from radiosonde measurements. These radiosonde launches, detailed by Holdridge (2020), occur multiple times a day at ARM sites, offering accurate but less frequent PBLH observations. For consistency in our methodology, we employ the Liu and Liang (2010) method to the LASSO output for PBLH calculations. This PBLH serves as the key parameter for calculating cloud-land coupling metrics.

Additionally, routine measurements of surface meteorological variables at the SGP site, including air temperature, relative humidity, and barometric pressure, are recorded at 10-min intervals. We use the Romps (2017)'s method to calculate the LCL from the surface meteorology. Lastly, observed surface sensible fluxes, available at a

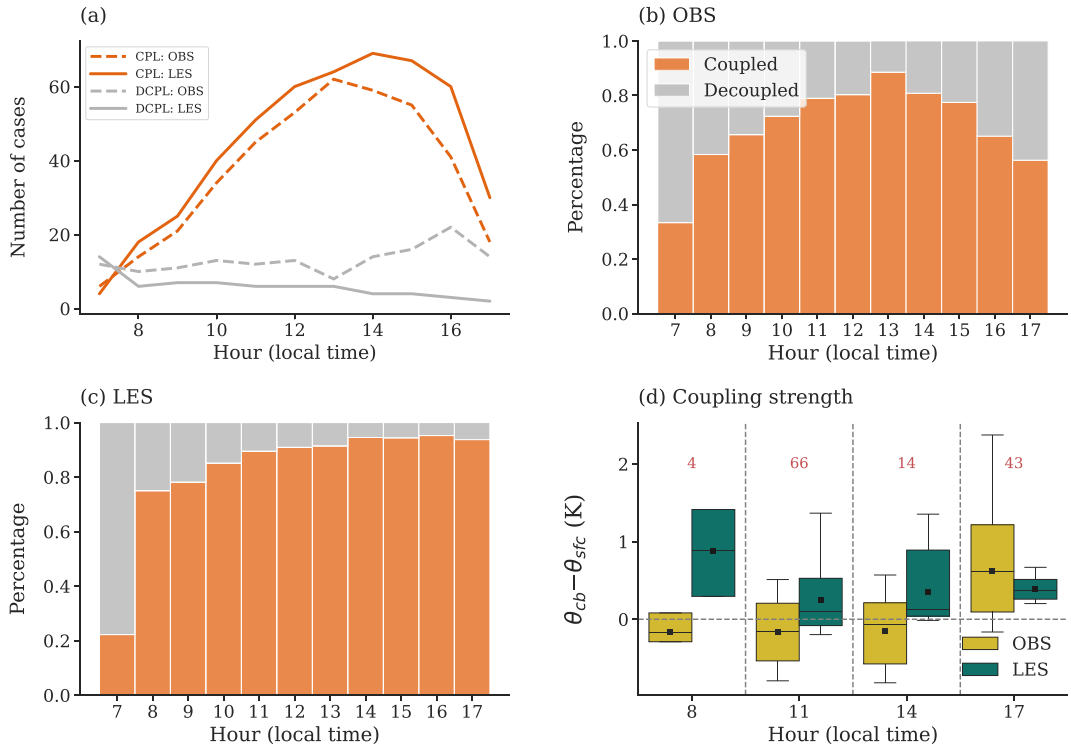

Figure 1. (a) Number of cases for coupled (orange curves) and decoupled (gray curves) clouds for each hour from observations (dashed curves) and Large-Eddy Simulation (LES) runs (solid curves). (b) Percentage of coupled-cloud and decoupled-cloud cases relative to their total count for each hour from observations. Panel (c) The same as panel (b), but from LES runs. (d) The strength of cloud-land coupling (defined as the difference in potential temperature between the cloud base and the surface) at four different hours from observations (yellow) and LES runs (green). The boxplot shows the10th, 25th, 50th, 75th, and 90th percentile values. The black square represents the mean value. The red number above shows the sampling number for each hour.

30-min resolution, are obtained from the Bulk Aerodynamic Energy Balance Bowen Ratio data product (BAEBBR; Wesely et al., 1995).

For comparison, all variables from both observations and model outputs used in this study are averaged up to a 1-hr value. These comprehensive data sets from different sources collectively provide a comprehensive approach to accurately assess PBLH, surface conditions, and their influence on cloud dynamics.

2.3. Coupling Metrics

For a coupled cloud-land system, turbulent fluxes generated from the land surface can reach the cloud base and affect the cloud development (i.e., surface fluxes, PBL, and cloud are coupled together via PBL turbulence). Otherwise, the cloud is decoupled from the surface (Su et al., 2023). To quantitively determine cloud-land coupling, the relative position of the cloud base to the PBL top or LCL is used. Following Su et al. (2022), a cloud deck is considered coupled from the surface if it satisfies any of the two following criteria: $\overline{\mathrm{CBH}} < \overline{\mathrm{PBLH}} + 0.2$ km or $\overline{\mathrm{CBH}} < \overline{\mathrm{LCL}} + 0.15$ km, where the overbar denotes the hourly mean. $\overline{\mathrm{CBH}}$ is set to be smaller than 4 km due to our focus on shallow clouds. For observations, the PBLH is lidar-derived. Su et al. (2022) have shown that the coupling metric retrieved from lidar demonstrates good consistency with those derived from radiosonde within about a 10% difference. Should neither of the conditions be satisfied, the cloud is regarded as decoupled from the surface. The number of coupled and decoupled cases for each hour from observations and LES runs is summarized in Figure 1a.

In addition to the identification of cloud-land coupling, the static stability of sub-cloud layers is used to determine the strength or degree of cloud-land coupling, calculated as the difference in potential temperature between the cloud base and the surface. The larger the stability is, the less the cloud is coupled from the surface.

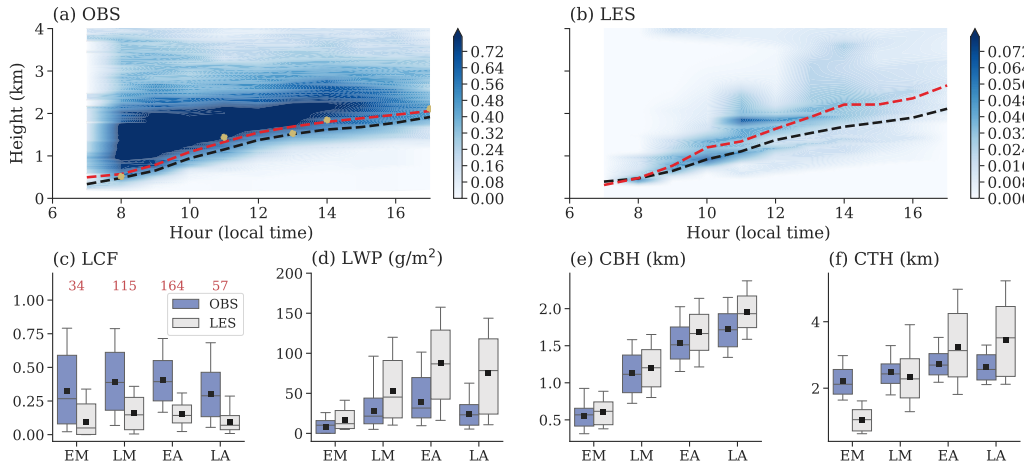

Figure 2. Time-height cross sections of cloud fraction averaged for the 77 case days under coupled conditions from (a) observations and (b) Large-Eddy Simulation (LES) runs. The red and black dashed lines represent the boundary-layer height (lidar-derived for observations and the Liu and Liang (2010) method for LES runs) and the lifted condensation level, respectively. Yellow dots denote the radiosonde-derived planetary boundary-layer height. Panel (c) presents comparisons of low-cloud fraction (LCF) between observations (blue) and LES runs (gray) for coupled clouds. LCF is sorted into four periods: Early Morning (EM, 0600–0900), Late Morning (LM, 0900–1200), Early Afternoon (EA, 1200–1500), and Late Afternoon (LA, 1500–1800). For each period, the left boundary is included, with the right excluded. The boxplot shows the 10th, 25th, 50th, 75th, and 90th percentile values. The black square represents the mean value. The red number denotes the sampling count for each period. Panels (d, f) are the same as panel (c), but for in-cloud liquid water path, cloud-base height, and cloud-top height, respectively.

3. Results

3.1. Occurrence Frequency of Coupled Cumulus Clouds

Figures 1b and 1c compare the evolution of the occurrence frequency of coupled and decoupled clouds (referencing their total count) between observations and LES runs. From observations, an evident diurnal cycle is observed in the frequency of coupled clouds (see orange bars in Figure 1b): lowest in the early morning, increasing steadily throughout the morning hours, reaching a peak around 1300 Local Time (LT; UTC − 6 hr), then gradually declining during the afternoon. The observed diurnal cycle of the coupled cloud frequency aligns with the variations in surface sensible heat fluxes (SHF) (Figure S4 in Supporting Information S1). However, LES runs do not capture this feature: They display a sharp increase in coupled cloud frequency in the early morning, followed by a gradual rise in the later morning hours, and then a consistent leveling off throughout the afternoon (Figure 1c). In other words, LES runs only correctly capture the surface-heat-driven variations in coupled cloud frequency in the morning, missing this feature in the afternoon. Moreover, the frequency of coupled clouds is significantly overestimated in LES runs, especially in the afternoon.

Figure 1d illustrates the evolution of cloud-land coupling strength, measured by the stratification of sub-cloud layers. More destabilized (stratified) sub-cloud layers represent a more coupled (decoupled) cloud-land system. Observations show no significant changes in coupling strength in the morning, followed by a significant decrease later in the day. This variation in the afternoon is consistent with the observed trend in coupled cloud frequency. However, as opposed to the observed decreasing trend, an insignificant change in coupling strength during the afternoon is mistakenly represented by LES runs.

3.2. Evaluation of Coupled Cloud Properties

In this section, we mainly focus on evaluations of cloud properties under coupled conditions, given too few decoupled cloud cases in the data set (Figure 1a). Figures 2a and 2b compare the evolution of cloud fraction of coupled cumulus between observations and LES runs. According to observations, cloud layers are lowest but thickest in the morning (Figure 2a). With sunrise, clouds start developing throughout the day, manifested by an increasingly rising cloud base. Meanwhile, the CTH does not change significantly, leading to a reduced cloud thickness over time. It should be noted that Figure 2 averages only the coupled cloudy cases. The average of

coupled cloudy cases during the morning tends to include stratiform clouds rather than the shallow cumulus clouds that develop throughout the daytime (Su, Li, Henao, et al., 2024). Stratiform clouds are typically characterized by relatively high and stable cloud tops, which explains the observed relatively constant CTH in the morning. In contrast, LES runs can generally capture the rising trend in the CBH (Figure 2b). However, other cloud properties are not properly represented in LES. For example, cloud fraction is significantly underestimated all day, and variations in cloud thickness are opposite to those observed, with thicker cloud layers simulated in the afternoon.

A thorough examination of the simulated cloud properties (LCF, in-cloud LWP, CBH, and CTH) for coupled cumulus clouds is presented in Figures 2c–2f. These properties are sorted into four three-hour intervals from 0600 LT to 1800 LT for a robust comparison: early morning (EM), late morning (LM), early afternoon (EA), and late afternoon (LA). The observed LCF's inverted V-shaped pattern, peaking in the LM or EA, is well captured by LES runs, although LCF is significantly underestimated by the model throughout the day (Figure 2c). These results hold when examining observed LCF by the total-sky imager (Morris, 2005) that provides retrievals of fractional sky cover (Figure S5 in Supporting Information S1). In terms of LWP, observations and LES runs exhibit a similar inverted V-shaped pattern (Figure 2d), but LES runs notably overestimate LWP in the afternoon, suggesting an exaggerated simulation of shallow convection. The misrepresentation of overshooting shallow convection is further corroborated by the overestimated CTH (Figure 2f). It is noted that insect contamination in ARSCL causes an overestimation of CTH, indicating that LASSO simulations may exaggerate the vertical extent of afternoon cumulus clouds more severely than what is observed in reality. Compared to other variables, the simulated CBH aligns relatively well with observations (Figure 2e).

3.3. Misrepresented PBL Processes

Our analyses revealed notable biases in cloud properties such as the overestimated LWP and CBH in the afternoon, which coincide with an overstated probability of coupled cloud occurrence. These discrepancies appear to stem from erroneous PBL simulations, indicated by concurrently overestimated PBLH (Figure 2a vs. Figure 2b, or Figure 4b). Figure 3 shows the relationship between observed (or simulated) cloud properties and their corresponding PBLHs under coupled conditions in the afternoon. No significant correlations are seen between LCF and PBLH in both observations and simulations (Figures 3a and 3b), suggesting that the bias in simulated LCF is not related to misrepresented PBLH development (Figure 3c). This warrants further investigation. However, a significant correlation is noticed between LWP and PBLH (Figure 3d), which is more pronounced in LES runs (Figure 3e). This indicates that the overestimation of LWP is associated with the exaggerated PBLH (Figure 3f), also true for the overestimated CTH (Figures 3g–3i).

The overestimated PBLH is possibly related to the effect of surface forcings. In LES runs, the PBL development is subject to the interplay between PBLH, turbulent kinetic energy (TKE), and surface fluxes (Figure S8 in Supporting Information S1): Increased surface fluxes (mainly SHF) drive stronger buoyancy fluxes within the PBL. These buoyancy fluxes predominantly contribute to the production of the TKE, whose increase finally prompts a rise in the PBLH. Due to the limited observed variables, we cannot examine these processes against observations stepwise. As a surrogate, we skip the intermediate physical processes and directly evaluate the responses of the PBLH to SHF. Figure 4a compares the PBLH versus the cumulative SHF from 1000 LT to 1700 LT between the model and observations, demonstrating that the PBLH is more sensitive to SHF variations in LES runs than in observations. This suggests that the LES model, given the same increment of sensible heat, tends to drive stronger PBL turbulence and more vigorous PBL development.

The enhanced efficiency of surface fluxes in driving PBL turbulence facilitates easier triggering of convection in the afternoon, potentially elucidating the higher frequency of coupled clouds in LES runs. The easier convective trigger is supported by Figure S6 in Supporting Information S1, showing a substantially larger value in (PBLH − LCL) in LES runs during the afternoon, where (PBLH − LCL) generally represents the tendency of the convective trigger (Wei et al., 2023). Because a convective cloud updraft tends to form if the cloud-initiating parcel reaches the LCL (Deng et al., 2003), the vertical velocity of the initial parcel (related to TKE in the PBL) and LCL are the two dominant factors that influence the convective trigger. To facilitate its comparison, PBLH is used as a surrogate for TKE, with the near-surface relative humidity (RH_{sfc}) for LCL because simulation biases of LCL are dictated by those of RH_{sfc} in the afternoon (see Figures S7a–c in Supporting Information S1). In

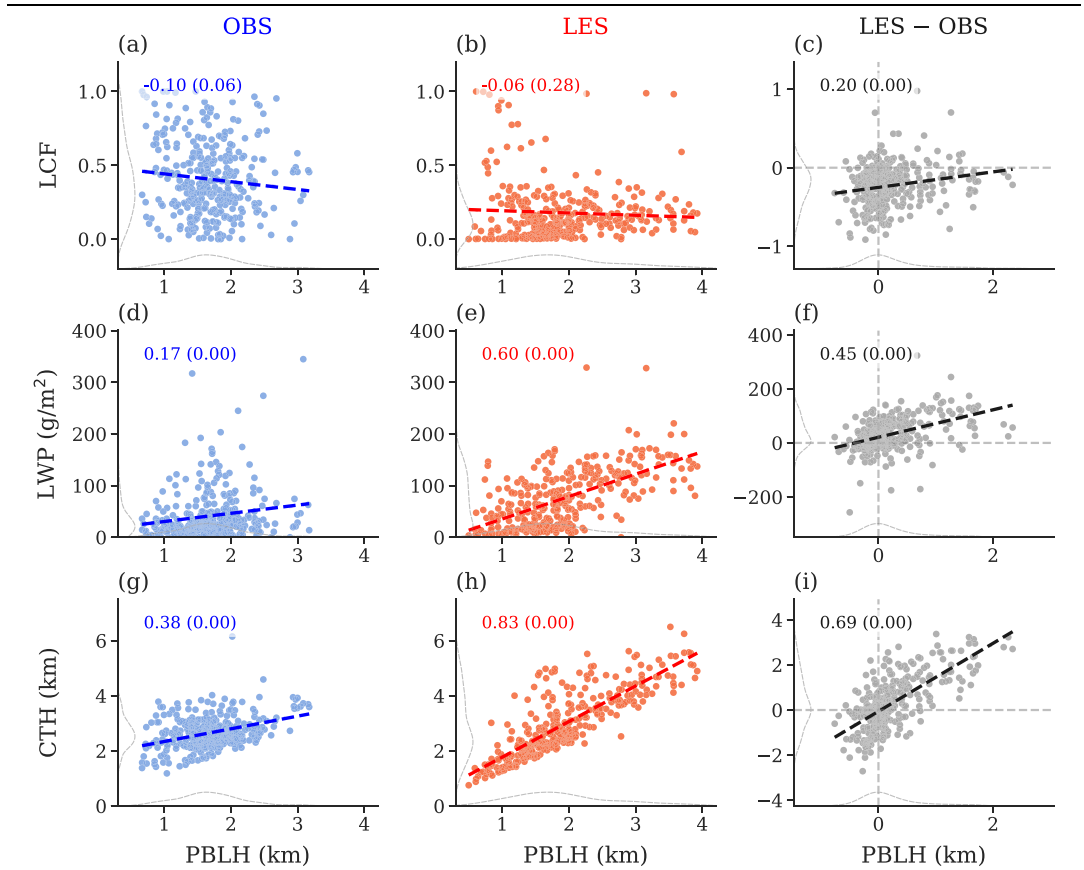

Figure 3. Scatter plots of low-cloud fraction (LCF) versus planetary boundary-layer height (PBLH) from 1000 LT to 1700 LT from (a) observations, (b) Large-Eddy Simulation (LES) runs, and (c) LES runs minus observations, respectively. The dashed line in each panel is the best-fit line from linear regression. The unbracked number is the correlation coefficient between LCF and PBLH, with the p-value shown in brackets. The gray dashed lines near the axes show the probability density functions of variables LCF and PBLH. The other two rows are the same as the first row but for liquid water path and cloud-top height.

that regard, the triggering of shallow convection can be represented by ϕ(PBLH, RH_{sfc}), where ϕ is a trigger function.

Figures 4c and 4d compare cloud occurrence frequencies as a function of PBLH and RH_{sfc} (ϕ) between LES runs and observations. Consistent with conventional wisdom, clouds are overall more easily triggered in humid and turbulent environments (Figure 4c). This phenomenon is well captured by LES runs (Figure 4d). However, clouds are triggered less in drier and more stable environments (indicated by dark colors), while significantly triggered more in turbulent conditions (highlighted by yellow colors). The latter well explains the LES runs' tendency to overestimate the frequency of coupled cloud occurrences in the afternoon when the PBL becomes more turbulent. The easier trigger of afternoon shallow convection in LES runs indicates a tighter coupling between the PBL, clouds, and the land surface. This excessive coupling strength partly arises from the high sensitivity of the PBL TKE to SHFs, which could be mitigated by reducing the coefficient for the surface-heat-flux term in the TKE budget equation. Additionally, the simplification of the land model in LES runs by prescribing surface fluxes contributes to this issue. It fails to consider the dynamic negative feedback of increased LWP on surface energy (surface shading by clouds), which typically weakens shallow convection. Furthermore, this simplification overlooks the roles of surface heterogeneity and cloud-shadow-induced dynamic heterogeneity in land-atmosphere interactions, exacerbating LWP overestimation (Xiao et al., 2018).

4. Summary

This study constitutes a preliminary assessment of cloud-land coupling in the LASSO LESs (LES), focusing on 77 case days with shallow convection. Our examination delves into cloud-land coupling processes, contrasting

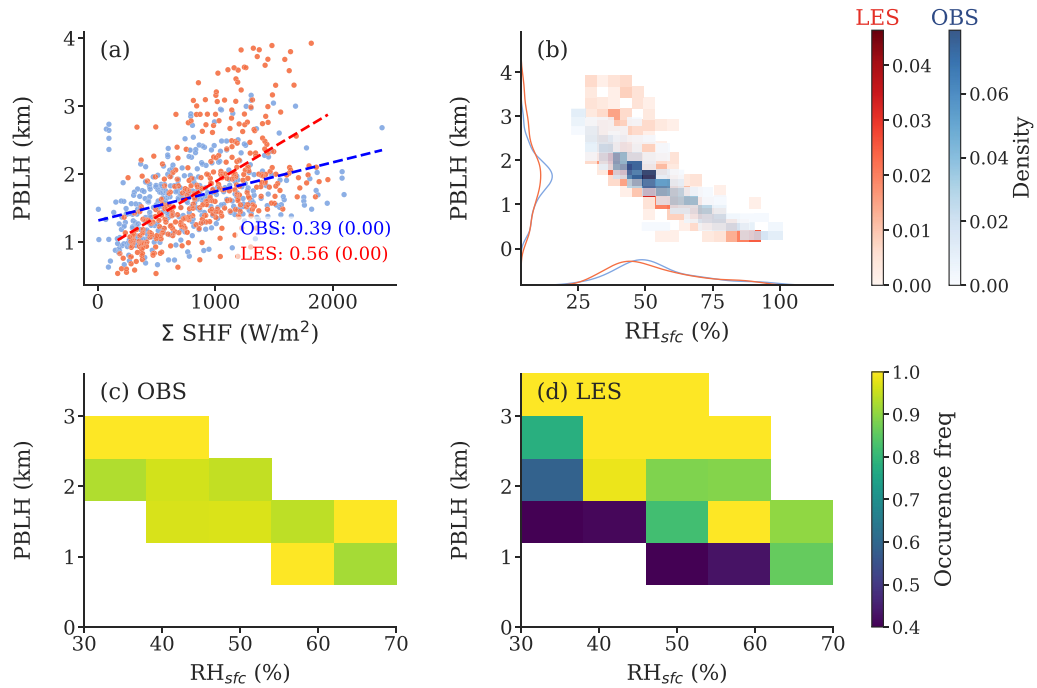

Figure 4. (a) Scatter plot of planetary boundary layer height (PBLH) versus cumulative sensible heat fluxes (SHF) (starting from 0600 LT; Σ SHF) from 1000 LT to 1700 LT between observations (blue) and Large-Eddy Simulation (LES) runs (red). The dashed lines are the best-fit lines from linear regression. Unbracketed numbers are correlation coefficients between PBLH and Σ SHF, with p-values shown in brackets. (b) Joint probability density functions (PDFs) of the PBLH and the near-surface relative humidity (RH_{sfc}) between LES runs (red) and observations (blue). The solid lines near the axes show the PDFs of the PBLH or RH_{sfc}. Panels (c), (d) show cloud occurrence frequencies corresponding to PBLH and RH_{sfc} from 1000 LT to 1700 LT for observations and LES runs, respectively. For each case, cloud occurrence is determined when the low-cloud fraction exceeds 0.02.

LES simulations with observations. The diurnal patterns of coupled cloud occurrence in observations are closely tied to local time and diurnal variations of surface fluxes. LES runs can broadly capture this evolution but overestimate coupled cloud occurrences in the afternoon, mirrored by the overprediction of cloud LWP and the vertical extent of cumulus clouds. These overestimated cloud properties are found to be related to a more vigorous PBL simulated by LES runs. The overestimation of coupled cloud occurrence frequency in the afternoon is likely caused by a more efficient trigger of shallow convection represented in the LES model, given the same level of turbulent energy and moisture background. This highlights a deficiency in the representation of cloud-land interactions and boundary layer processes. One potential limit of our study is that we did not examine the sensitivity of the results to the choice of microphysics schemes, which might affect cloud-surface coupling by changing precipitation. It warrants further investigation. This study underscores the crucial need to enhance cloud-land coupling in LESs, possibly through decreasing the coefficient for the surface-heat-flux term in the TKE budget equation or employing an interactive land surface model, as discussed in Section 3.3. Improvements in cloud-surface coupling will not only help increase the accuracy of cloud simulations in future LASSO experiments but also refine the representation of cloud-aerosol interactions near the surface, considering the influence of coupling on the PBL vertical mixing of aerosols.

Data Availability Statement

Model outputs from LASSO LESs and observed cloud properties derived from ARSCL and COGS data sets over the SGP are available at the LASSO bundle browser (Gustafson, Vogelmann, Cheng, et al., 2020). ARM radiosonde data are available at Holdridge (2020). Surface SHF are from the Bulk Aerodynamic Energy Balance Bowen Ratio data product (Zhu et al., 2023). PBLH data derived in this study and model configurations for selected case days in ID1-5 are available at Zhang et al. (2024).

Acknowledgments
This study is supported by the Department of Energy (DOE) Atmospheric System Research program (DESC0022919) and the National Science Foundation (AGS2126098). YZ is supported by the DOE Early Career Grant (DE-SC0024185). T. Su is supported by the DOE Atmospheric System Research Science Focus Area THREAD project. Work at the Lawrence Livermore National Laboratory is performed under the auspices of the U.S. DOE by LLNL under Contract DE-AC52-07NA27344. The authors thank two anonymous reviewers for their constructive comments, which considerably improved the quality of the manuscript, and Maureen Cribb for editing this manuscript.

References

Angevine, W. M., Olson, J., Kenyon, J., Gustafson, W. I., Endo, S., Suselj, K., & Turner, D. D. (2018). Shallow Cumulus in WRF parameterizations evaluated against LASSO large-eddy simulations. *Monthly Weather Review*, *146*(12), 4303–4322. https://doi.org/10.1175/MWR-D-18-0115.1

Basu, S., Holtslag, A. A. M., Wiel, B. J. H., Moene, A. F., & Steeneveld, G. J. (2008). An inconvenient "truth" about using sensible heat flux as a surface boundary condition in models under stably stratified regimes. *Acta Geophysica*, *56*(1), 88–99. https://doi.org/10.2478/s11600-007-0038-y

Bretherton, C. S., & Wyant, M. C. (1997). Moisture transport, lower-tropospheric Stability, and decoupling of cloud-topped boundary layers. *Journal of the Atmospheric Sciences*, *54*(1), 148–167. https://doi.org/10.1175/1520-0469(1997)054<0148:MTLTSA>2.0.CO;2

Catalano, F., Alessandri, A., De Felice, M., Zhu, Z., & Myneni, R. B. (2016). Observationally based analysis of land-atmosphere coupling. *Earth System Dynamics*, *7*(1), 251–266. https://doi.org/10.5194/esd-7-251-2016

Clothiaux, E. E., Ackerman, T. P., Mace, G. G., Moran, K. P., Marchand, R. T., Miller, M. A., & Martner, B. E. (2000). Objective determination of cloud heights and radar reflectivities using a combination of active remote sensors at the ARM CART sites. *Journal of Applied Meteorology*, *39*(5), 645–665. https://doi.org/10.1175/1520-0450(2000)039<0645:ODOCHA>2.0.CO;2

Deng, A., Seaman, N. L., & Kain, J. S. (2003). A shallow-convection parameterization for mesoscale models. Part I: Submodel description and preliminary applications. *Journal of the Atmospheric Sciences*, *60*(1), 34–56. https://doi.org/10.1175/1520-0469(2003)060<0034:ASCPFM>2.0.CO;2

Dickinson, R. E. (1995). Land-atmosphere interaction. *Reviews of Geophysics*, *33*(2 S), 917–922. https://doi.org/10.1029/95RG00284

van der Dussen, J. J., De Roode, S. R., Gesso, S. D., & Siebesma, A. P. (2015). An LES model study of the influence of the free tropospheric thermodynamic conditions on the stratocumulus response to a climate perturbation. *Journal of Advances in Modeling Earth Systems*, *7*(2), 670–691. https://doi.org/10.1002/2014MS000380

van der Dussen, J. J., De Roode, S. R., & Siebesma, A. P. (2014). Factors controlling rapid stratocumulus cloud thinning. *Journal of the Atmospheric Sciences*, *71*(2), 655–664. https://doi.org/10.1175/JAS-D-13-0114.1

Entekhabi, D. (1995). Recent advances in land-atmosphere interaction research. *Reviews of Geophysics*, *33*(2 S), 995–1003. https://doi.org/10.1029/95RG01163

Fairless, T., Vogelmann, A., Johnson, K., Gustafson, W., Oktem, R., & Romps, D. (2021). LASSO shallow cumulus cases evaluated with the Clouds Optically Gridded by Stereo (COGS) product. In *2021 Joint ARM user facility and ASR PI meeting*. Retrieved from https://www.arm.gov/meetings/stm/posters/pdf/2021/P002746.pdf

Gustafson, W., Vogelmann, A., Cheng, X., Dumas, K., Endo, S., Johnson, K., et al. (2020). Description of the LASSO data bundles product [Dataset]. https://doi.org/10.2172/1469590

Gustafson, W. I., Vogelmann, A. M., Cheng, X., Endo, S., Krishna, B., Li, Z., et al. (2018). Description of the LASSO alpha 2 release. https://doi.org/10.2172/1376727

Gustafson, W. I., Vogelmann, A. M., Li, Z., Cheng, X., Dumas, K. K., Endo, S., et al. (2020). The large-eddy simulation (LES) atmospheric radiation measurement (ARM) symbiotic simulation and observation (LASSO) activity for continental shallow convection. *Bulletin of the American Meteorological Society*, *101*(4), E462–E479. https://doi.org/10.1175/BAMS-D-19-0065.1

Holdridge, D. (2020). Balloon-borne sounding system (SONDE) instrument handbook [Dataset]. https://www.arm.gov/capabilities/instruments/sonde

Liu, S., & Liang, X. Z. (2010). Observed diurnal cycle climatology of planetary boundary layer height. *Journal of Climate*, *23*(21), 5790–5809. https://doi.org/10.1175/2010JCLI3552.1

Morris, V. R. (2005). *Total sky imager handbook*. Tech. Rep. ARM TR-017. Retrieved from https://www.arm.gov/publications/tech_reports/handbooks/tsi_handbook.pdf

Nicholls, S. (1984). The dynamics of stratocumulus: Aircraft observations and comparisons with a mixed layer model. *Quarterly Journal of the Royal Meteorological Society*, *110*(466), 783–820. https://doi.org/10.1002/qj.49711046603

Nicholls, S., & Leighton, J. (1986). An observational study of the structure of stratiform cloud sheets: Part II. Entrainment. *Quarterly Journal of the Royal Meteorological Society*, *112*(472), 431–460. https://doi.org/10.1002/qj.49711247209

Qian, Y., Huang, M., Yang, B., & Berg, L. K. (2013). A modeling study of irrigation effects on surface fluxes and land – Air – cloud interactions in the Southern Great Plains. *Journal of Hydrometeorology*, *14*(3), 700–721. https://doi.org/10.1175/JHM-D-12-0134.1

Romps, D. M. (2017). Exact expression for the lifting condensation level. *Journal of the Atmospheric Sciences*, *74*(12), 3891–3900. https://doi.org/10.1175/JAS-D-17-0102.1

Romps, D. M., & Öktem, R. (2018). Observing clouds in 4d with multiview stereophotogrammetry. *Bulletin of the American Meteorological Society*, *99*(12), 2575–2586. https://doi.org/10.1175/BAMS-D-18-0029.1

Sandu, I., Stevens, B., & Pincus, R. (2010). On the transitions in marine boundary layer cloudiness. *Atmospheric Chemistry and Physics*, *10*(5), 2377–2391. https://doi.org/10.5194/acp-10-2377-2010

Santanello, J. A., Dirmeyer, P. A., Ferguson, C. R., Findell, K. L., Tawfik, A. B., Berg, A., et al. (2018). Land–atmosphere interactions: The LoCo perspective. *Bulletin of the American Meteorological Society*, *99*(6), 1253–1272. https://doi.org/10.1175/BAMS-D-17-0001.1

Sisterson, D. L., Peppler, R. A., Cress, T. S., Lamb, P. J., & Turner, D. D. (2016). The ARM Southern Great Plains (SGP) site. *Meteorological Monographs*, *57*(6), 1–6.14. https://doi.org/10.1175/amsmonographs-d-16-0004.1

Su, T., Li, Z., Henao, N. R., Luan, Q., & Yu, F. (2024). Constraining effects of aerosol-cloud interaction by accounting for coupling between cloud and land surface. *Science Advances*, *10*(21), eadl5044. https://doi.org/10.1126/sciadv.adl5044

Su, T., Li, Z., & Kahn, R. (2020). A new method to retrieve the diurnal variability of planetary boundary layer height from lidar under different thermodynamic stability conditions. *Remote Sensing of Environment*, *237*, 111519. https://doi.org/10.1016/j.rse.2019.111519

Su, T., Li, Z., Zhang, Y., Zheng, Y., & Zhang, H. (2024). Observation and reanalysis derived relationships between cloud and land surface fluxes across cumulus and stratiform coupling over the Southern Great Plains. *Geophysical Research Letters*, *51*(8). https://doi.org/10.1029/2023GL108090

Su, T., Li, Z., & Zheng, Y. (2023). Cloud-surface coupling alters the morning transition from stable to unstable boundary layer. *Geophysical Research Letters*, *50*(5). https://doi.org/10.1029/2022GL102256

Su, T., Zheng, Y., & Li, Z. (2022). Methodology to determine the coupling of continental clouds with surface and boundary layer height under cloudy conditions from Lidar and meteorological data. *Atmospheric Chemistry and Physics*, *22*(2), 1453–1466. https://doi.org/10.5194/acp-22-1453-2022

Tang, Q., Xie, S., Zhang, Y., Phillips, T. J., Santanello, J. A., Cook, D. R., et al. (2018). Heterogeneity in warm-season land-atmosphere coupling over the U.S. Southern Great Plains. *Journal of Geophysical Research: Atmospheres*, *123*(15), 7867–7882. https://doi.org/10.1029/2018JD028463

Trier, S. B., LeMone, M. A., Chen, F., & Manning, K. W. (2011). Effects of surface heat and moisture exchange on ARW-WRF warm-season precipitation forecasts over the central United States. *Weather and Forecasting*, *26*(1), 3–25. https://doi.org/10.1175/2010WAF2222426.1

Turner, D. D., Clough, S. A., Liljegren, J. C., Clothiaux, E. E., Cady-Pereira, K. E., & Gaustad, K. L. (2007). Retrieving liquid water path and precipitable water vapor from the atmospheric radiation measurement (ARM) microwave radiometers. *IEEE Transactions on Geoscience and Remote Sensing*, *45*, 3680–3689. https://doi.org/10.1109/TGRS.2007.903703

Wang, H., Rasch, P. J., & Feingold, G. (2011). Manipulating marine stratocumulus cloud amount and albedo: A process-modelling study of aerosol-cloud-precipitation interactions in response to injection of cloud condensation nuclei. *Atmospheric Chemistry and Physics*, *11*(9), 4237–4249. https://doi.org/10.5194/acp-11-4237-2011

Wei, J., Lu, B., Song, Y., Chen, H., & Weng, Z. (2023). Anthropogenic aerosols weaken land–atmosphere coupling over North China. *Geophysical Research Letters*, *50*(20). https://doi.org/10.1029/2023GL105685

Wesely, M. L., Cook, D. R., & Coulter, R. L. (1995). Surface heat flux data from energy balance Bowen ratio systems. Retrieved from https://www.osti.gov/biblio/69120

Xiao, H., Berg, L. K., & Huang, M. (2018). The impact of surface heterogeneities and land-atmosphere interactions on shallow clouds over ARM SGP site. *Journal of Advances in Modeling Earth Systems*, *10*(6), 1220–1244. https://doi.org/10.1029/2018MS001286

Xie, S., Cederwall, R. T., & Zhang, M. (2004). Developing long-term single-column model/cloud system-resolving model forcing data using numerical weather prediction products constrained by surface and top of the atmosphere observations. *Journal of Geophysical Research*, *109*(1). https://doi.org/10.1029/2003jd004045

Zhang, H., Su, T., Zheng, Y., & Li, Z. (2024). Dataset for paper titled "First assessment of cloud-land coupling in LASSO Large-Eddy Simulations" (v2.0) [Dataset]. *Zenodo*. https://doi.org/10.5281/zenodo.12556662

Zhang, H., Zheng, Y., Lee, S. S., & Li, Z. (2023). Surface-atmosphere decoupling prolongs cloud lifetime under warm advection due to reduced entrainment drying. *Geophysical Research Letters*, *50*(10). https://doi.org/10.1029/2022GL101663

Zhang, Y., & Klein, S. A. (2010). Mechanisms affecting the transition from shallow to deep convection over land: Inferences from observations of the diurnal cycle collected at the ARM Southern Great Plains site. *Journal of the Atmospheric Sciences*, *67*(9), 2943–2959. https://doi.org/10.1175/2010JAS3366.1

Zhang, Y., & Klein, S. A. (2013). Factors controlling the vertical extent of fair-weather shallow cumulus clouds over land: Investigation of diurnal-cycle observations collected at the ARM southern great plains site. *Journal of the Atmospheric Sciences*, *70*(4), 1297–1315. https://doi.org/10.1175/JAS-D-12-0131.1

Zheng, Y., Kumar, A., & Niyogi, D. (2015). Impacts of land–atmosphere coupling on regional rainfall and convection. *Climate Dynamics*, *44*(9–10), 2383–2409. https://doi.org/10.1007/s00382-014-2442-8

Zheng, Y.-T., Zhang, H., & Li, Z. (2021). Role of surface latent heat flux in shallow cloud transitions: A mechanism-denial LES study. *Journal of the Atmospheric Sciences*, *78*, 2709–2723. https://doi.org/10.1175/JAS-D-20-0381.1

Zheng, Y.-T., Zhang, H., Rosenfeld, D., Lee, S.-S. S., Su, T., & Li, Z. (2021). Idealized large-eddy simulations of stratocumulus advecting over cold water. Part I: Boundary layer decoupling. *Journal of the Atmospheric Sciences*, *78*(12), 4089–4102. https://doi.org/10.1175/JAS-D-21-0108.1

Zhu, W., Fan, L., & Jia, S. (2023). Integration of microwave satellite soil moisture products in the contextual surface temperature-vegetation index models for spatially continuous evapotranspiration estimation [Dataset]. *ISPRS Journal of Photogrammetry and Remote Sensing*, *203*, 211–229. https://doi.org/10.1016/j.isprsjprs.2023.08.004